To be submitted to
Physical Review

ISTITUTO NAZIONALE DI FISICA NUCLEARE
Laboratori Nazionali di Frascati

LNF-81/58(P)
8 Ottobre 1981

M. Capozi, S. Nannarone, G. Ottaviani, F. Patella, P. Perfetti, C. Quaresima and A. Savoia: LOW ENERGY ELECTRON LOSS SPECTROSCOPY (LEELS) AND AUGER ELECTRON SPECTROSCOPY STUDIES (AES) OF NOBLE METAL-SILICON INTERFACES: Si-Au SYSTEM

Servizio Documentazione
dei Laboratori Nazionali di Frascati
Cas. Postale 13 - Frascati (Roma)

INFN - Laboratori Nazionali di Frascati
Servizio Documentazione

LNF-81/58(P)
8 Ottobre 1981

LOW ENERGY ELECTRON LOSS SPECTROSCOPY (LEELS) AND AUGER ELECTRON SPECTROSCOPY STUDIES (AES) OF NOBLE METAL-SILICON INTERFACES: Si-Au SYSTEM

P. Perfetti, S. Nannarone, F. Patella, C. Quaresima, M. Capozi and A. Savoia
PULS-GNSM-INFN, Laboratori Nazionali di Frascati, 00044 Frascati, Italy

and

G. Ottaviani
Istituo di Fisica, Università di Modena and GNSM-CNR, 41100 Modena, Italy

ABSTRACT

We report complete LEELS and AES measurements on the Si(111) (2x1)-Au system at different thicknesses of Au deposited at room temperature and for different annealing cycles. Two overlayer thickness ranges correspond to two different stages of interface formation. In the submonolayer range gold atoms stick on the silicon surface without intermixing and give rise to strong interface LEELS features. A thickness of two monolayers is the lower limit over wich intermixing occurs and an Au-Si alloy is formed. The alloy composition changes with overlayer thickness up to 20 mL. Above this value pure gold begins to growth with some silicon outdiffused to the free surface. LEELS data show that in the alloyed phase the shallowest d-electrons are those mostly involved in bond formation with silicon-sp electrons. The hibrid bonds correspond to new electronic states at 3.7 eV under E_F for the silicon-rich Au-Si mixed phase.

1. INTRODUCTION

We report a complete set of LEELS and AES measurements on the Si(111)-Au system at different thicknesses of Au deposited at room temperature (RT). Both low ($\lesssim 1$ monolayer (mL)) and high Au coverages (up to 100 mL) have been explored and annealing cycles up to 500 °C have been performed on samples with different Au thicknesses. This work deal with the question of the interaction of the metal overlayer and the silicon substrate and the subsequent formation of an abrupt or diffuse interface. The existence of interface states as well as intermixed phase-electronic states will be examined in detail.

Gold is widely employed in mincroelectronics, e.g. for ohmic contacts and for schottky barriers[1]. The Si-Au system has been widely studied in the past. Only recently, however, a great insight into the physical problems connected to the interface formation has been reached with surface sensitive techniques such as Ultraviolet Photoemission Spectroscopy (UPS)[2,3,4], AES[5,6,7,8], Low Energy Electron Diffraction (LEED)[5,8] and

2. EXPERIMENTAL PROCEDURES

Clean silicon (111) 2x1 surface were obtained by cleaving a n-type silicon bar ($\varrho \simeq 0.05$ ohmxcm) in a ultrahigh vacuum chamber at a base pressure of the order of $1x10^{-10}$ torr. Notches on the bar allowed many cleaves without breaking the vacuum. Gold was deposited by thermal evaporation from a tungsten crucible. The evaporated film was step-by-step increased from a fraction of a monolayer to 100 mL. All the depositions were done with the silicon substrate at RT and the annealing cycles (see Sect. 3) were performed with a resistive heating system on the back of the sample holder. Great care was used in degassing the tungsten crucible to avoid contamination of the sample. During the depositions the vacuum pressure was always lower than $3x10^{-10}$ torr and no trace of contaminants was in the Auger spectra (sensitivity: 10^{-2} mL of carbon). The film thickness was measured by a piezoelettric monitor. The nominal one-monolayer coverage (θ=1) was defined as one Au atom per substrate atom (Si(111) surface density $\approx 7.8x10^{14}$ atoms/cm^{-2}), corresponding to a nominal thickness of 1.3 A. The electron energy Analyzer is a Physical Electronics double pass Cylindrical-Mirror (CMA) and its coaxial electron gun was used both for AES and LEELS spectroscopy. For LEELS the primary electron beam energy was lowered down to $\approx$ 100 eV and the angle of incidence was 45° with respect to the sample normal. A phase-sensitive detection system was used in the first and second derivative modes. Low-energy electron diffraction patterns were used to check the crystal structure of the clean and Au-covered silicon surfaces. The results here reported correspond to several different deposition sequences and/or annealing cycles. After some of these runs the surface morfology were investigated by SEM.

3. - RESULTS

3.1. Low-energy electron loss results

Fig. 1 gives a summary of different series of LEELS measurements. Each run corresponds to one of the full

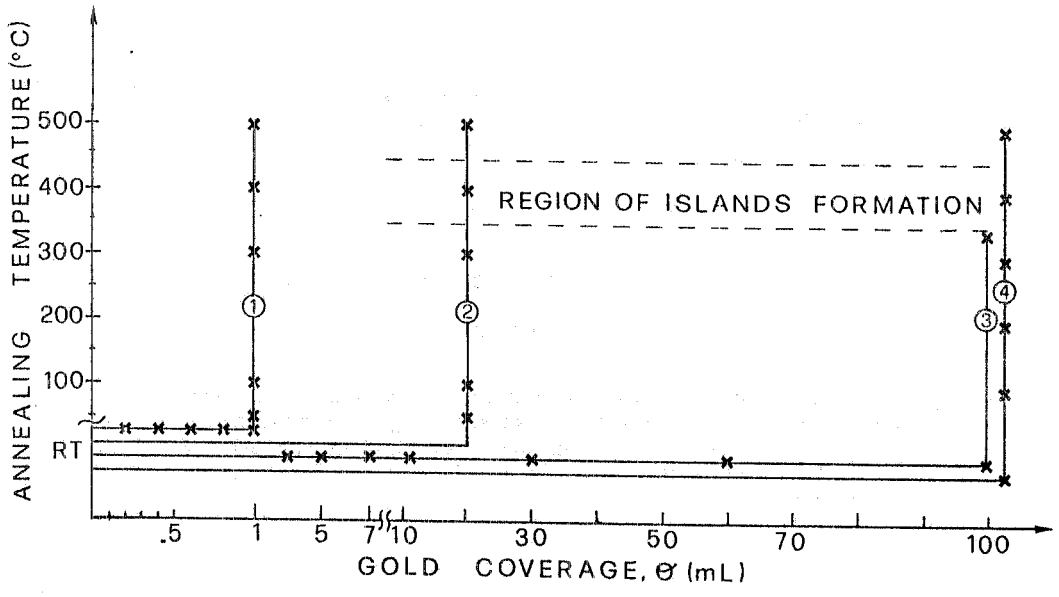

Fig. 1 - Each line corresponds to a different run identified by the reference number on the line. Each run consists of successive depositions at RT followed by annealing. The region were islands formation occurs is indicate by dashed lines.

lines and to the reference number on it. Each run consists of successive Au depositions followed by annealing. The annealing temperature and the coverage step were changed from run to run while the annealing time was 30 minutes. For each annealing step crosses on the full lines show the stage of each run at which LEELS, AES and LEED were performed.

LEELS curves for run 1 are reported in Fig. 2. The left side of the figure shows the evolution of the spectrum

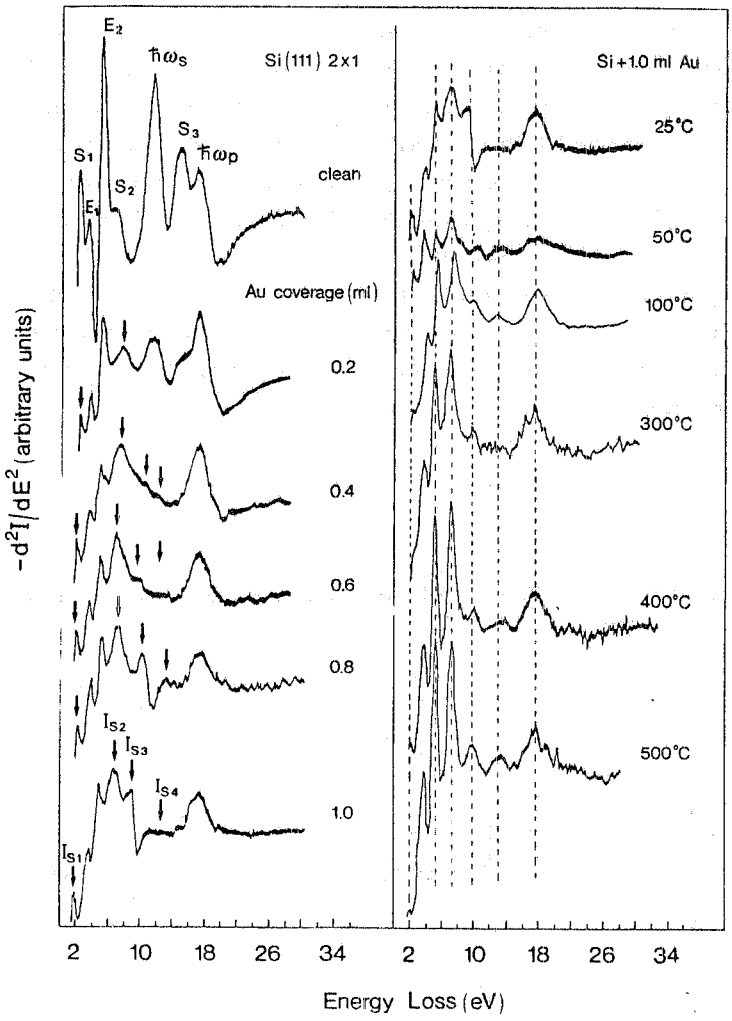

Fig. 2 - LEELS curves of clean cleaved Si(111) 2x1 and of the same surfaces covered with different thicknesses of gold (submonolayer coverage). The right-hand side of the figure shows the spectra obtained after 30 minutes of annealing at different temperatures for 1 mL coverage.

for increasing Au coverages in the submonolayer region. The right side of the same figure shows the effects of the annealing. The first left-side spectrum corresponds to clean Si(111) and all the features have been previously identified. In particular the peaks at 16.9 eV and 11.0 eV correspond to bulk and surface plasmon losses. Peaks E_1 at 3.6 eV and E_2 at 5.2 eV are one-electron transitions related to the bulk-Si band structure. The remaining losses S_1, S_2 and S_3 at 2.4 eV, 6.9 eV and 15.1 eV involve transitions between back-bond surface states and empty

surface states. A small amount of gold cause a strong modification of the spectrum. The surface losses disappear at 0.4 mL coverage. A new structure I_{S2} appear at 7.6 eV for a 0.2 mL coverage. Its position shifts to 7.0 eV at 0.6 mL and it does not change for higher coverages. We interpret the structure I_{S1} at 2.2 eV as a gold-induced feature rather than a surviving S_1 peak since the S_1 transition which involves the Si dangling bonds is removed by very small amount of deposited materials[16]. As we shall see later the peaks I_{S1}, I_{S2}, I_{S3}, I_{S4} are observed at low coverages and they disappear at higher coverages therefore we interpret them as interface features. An interesting result shown on the right-hand side of Fig. 2 is that each 30-minutes annealing step does not change the peak positions up to 500°C. The most striking effect of temperature is the narrowing of all the spectral features. The above results are summarized by Fig. 3 where the energy of the LEELS features is shown as a

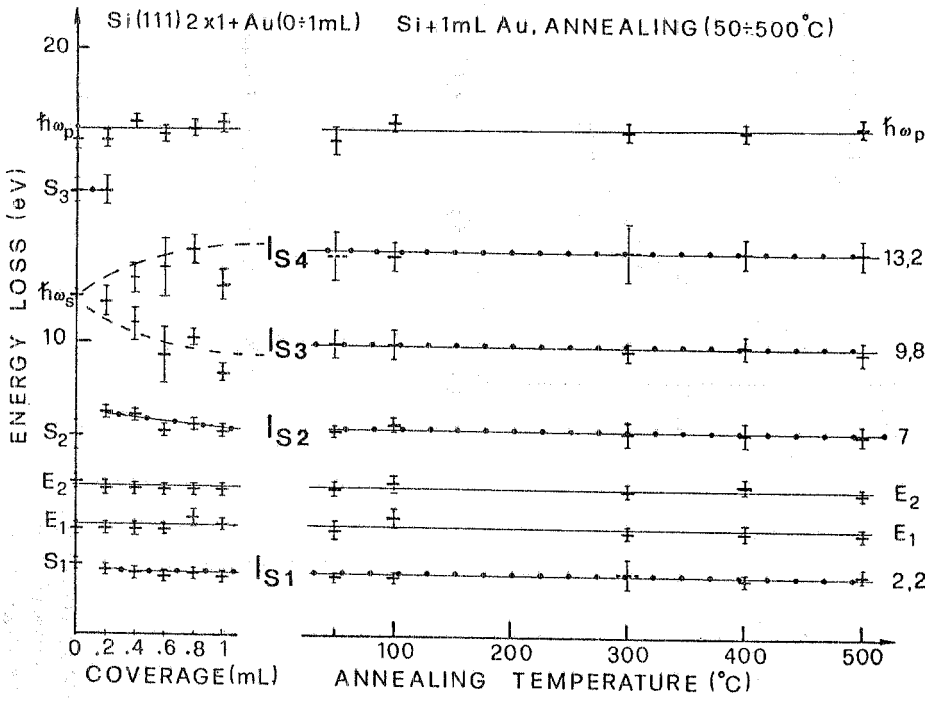

Fig. 3 - Energy positions of LEELS features vs. Au coverage and annealing temperature. Dots on full lines indicate surface and interface losses. Dashed lines are the best fit of Eq.(6) to the experimental results (see text).

function of coverage and annealing temperature. The sharp 2x1 LEED pattern of the Si(111) cleaved face becames weak at 1 mL coverage and it completely disappeared at higher coverages.

In Fig. 4 we report the results of run 3. Here the Au coverage was incrased by large increments to follow the evolution of spectra until the pure gold-like situation is reached at 100 mL. Notice that the energy resolution was slightly worst here than for the other runs. The broad low-energy peak at θ=2 correspond to the double peak at θ=5. The evolution saturates at θ=12-30 when all new structures B, C, D, E, F are well developed. Peak B is already well defined for θ=5 and its energy position is 3.7 eV. For higher coverages it shifts to lower energy and reaches its final position, 2.5 eV, around θ=30. The other structures C, D, E, F at 6 eV, 11 eV, 16 eV and 22 eV remain unchanged above θ=12. Fig. 5 shows the energy position of peak B as a function of Au-coverage. The observed shift cannot be attributed to a background effect. In fact the same effect should otherwise be seen also for peak C.

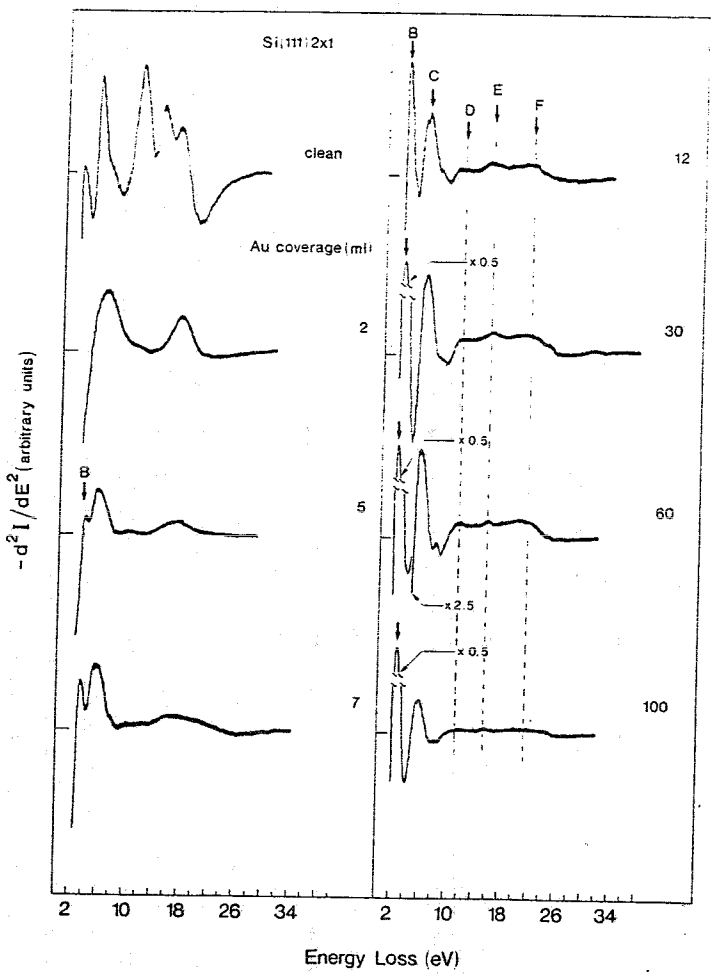

Fig. 4 - LEELS curves for clean cleaved silicon (111) 2x1 and for the same surface covered with different Au thickness. The Au coverage is increased by large increments up to $\theta = 100$.

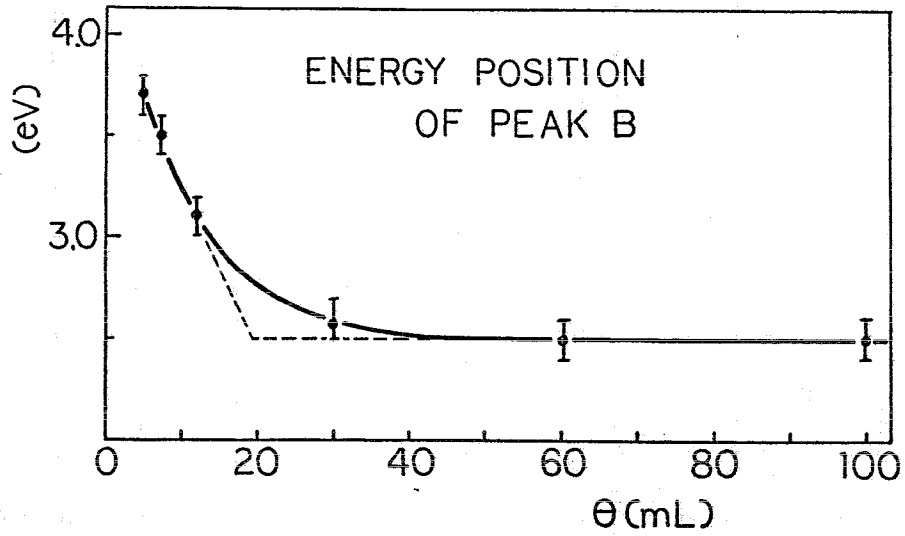

Fig. 5 - Energy position of peak B vs. the Au coverage.

We have seen in Fig. 2 that one monolayer of gold forms a stable system--no changes in the LEELS spectrum are caused by the annealing processes. We will show now that this stability depends on the gold thickness. The effects of the annealing cycles for a 20 mL thick Au overlayer are reported in Fig. 6. In the RT spectrum peak C seems now a convolution of two different peaks. Peaks E and F are less evident in Fig. 6 than in Fig. 4. The effects of annealing are dramatics in Fig. 6 and the spectrum is completely changed at the end of the annealing cycle. The peak evolution is more clear from Fig. 7. After 100°C peaks C and D are well splitted and evolve into four structures at 5.4 eV, 7.0 eV, 10.6 eV and 13.0 eV. Peak B rises slightly in energy and at 400°C it has the same energy as peak E_1 in the clean silicon. The bulk silicon plasmon reappears at 400°C and all the structures at 500°C correspond to those seen for the θ=1 spectrum, Fig. 2. Similar results are shown for run 4 in Figs. 8 and 9. Here the annealing process again splits both peaks D and C and the 500°C annealing step restablish the θ=1 spectrum. The major difference between run 2 and run 4 is that the splitting of peaks D and C occurs at higher temperatures for the latter run.

3.2. - Auger-Spectroscopy Results

The Auger processes involving the valence band yield information about the local density of states of the ionized atom if the Coulomb interaction between the two holes is small compared to the bandwidth[17,18,19]. This is the case of the Si LVV Auger transition. Therefore the single peak observed at 92 eV (see Fig. 10) is interpreted as a self-convolution of the partial sp density of states. Therefore the modifications of the Si LVV lineshape observed in Fig. 10 probe the involvement of Si p-like states in the substrate-overlayer chemical bond. One monolayer of Au gives an Au OVV peak at 69 eV and in the submonolayer range it affects only the intensity of the silicon peak. At θ=5 the gold structure becomes dominant and the Si-LVV feature splits into two peaks at 90 eV and 95 eV. This spectrum does not change for larger coverages except for the relative intensity of its two components. A striking effect is the persistency in the spectrum of the Si doublet up to at least θ=100. The intensity ratio Au:OVV/Si:LVV is shown in Fig. 11 as a function of θ. The ratio exhibits a continous increase wich saturates at $\theta \gtrsim 20$. In the inset of Fig. 11 the intensity ratio vs. θ plot is shown in detail for the submonolayer region. A linear behavior is observed for $\theta \leq 1$. The evolution of the low-energy Auger spectrum for θ=20 is shown in Fig. 12 as a function of annealing. The double silicon peak characteristic of θ=20 undergoes a strong change and it reaches its final single-peak lineshape between 400°C and 500°C. Similar results were obtained for θ=100 after the same annealing cycle. The intensity ratio between the Si-KLL and the Au-MNN Auger peaks for the annealing cycles of the 20 mL and 100 mL coverages are shown in Fig. 13 together with the Au:OVV/Si:LVV of θ=1. The study of the high-energy Auger lines is complementary to that of lines involving the valence band. In fact intermixing processes between gold and silicon strongly influence the valence band states while they weakly affects the core levels. Therefore the interpretation of the spectra becomes simpler in the latter case.

3.3. - Surface Morfology

The surface morfology has been investigated with a scanning electron microscope. The analysis has been performed mainly on samples covered with 100 mL of gold. In the samples as deposited no particular features have been observed and the gold film appears quite continuous. After annealing at temperatures higher than 350-400°C gold islands are formed, as shown in Fig. 14. The islands are different in shape with an average height of 1 μm and a bottom area of the order of few μm^2. The percentage of the area covered by the islands is 10% of the total sample area. In Fig. 14 is reported a sketch showing islands connected with a thin gold film. The presence of such a thin film cannot be proved by SEM but only inferred from AES and LEELS results, previously presented. The composition of the islands has been studied with X ray diffraction technique. They are substantially gold with dissolved at maximum few percent of silicon. No evidence for compounds has been found.

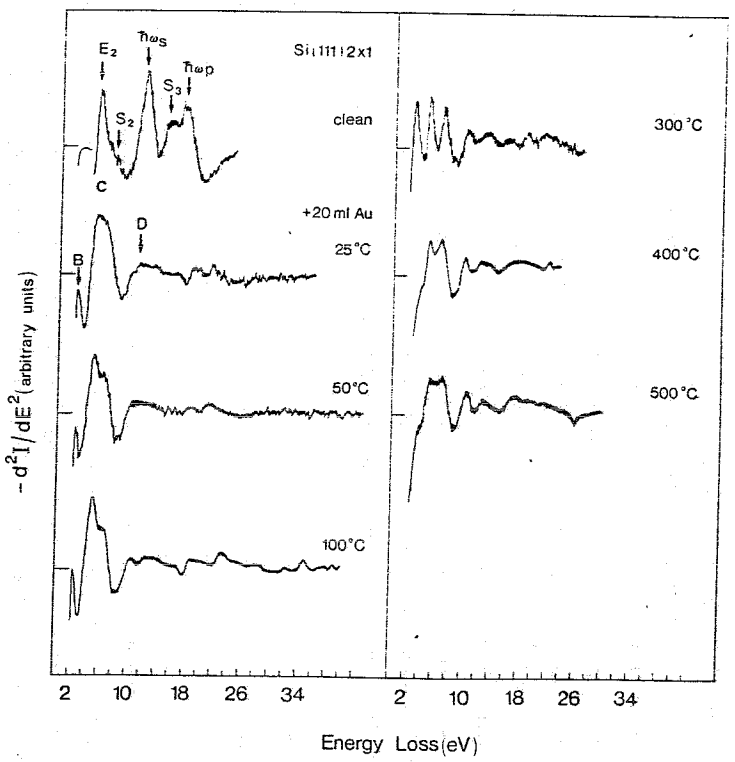

Fig. 6 - LEELS spectra for θ = 20 at RT and after different 30-minutes annealing steps at different temperatures. The top left spectrum is that of clean cleaved Si(111) 2x1.

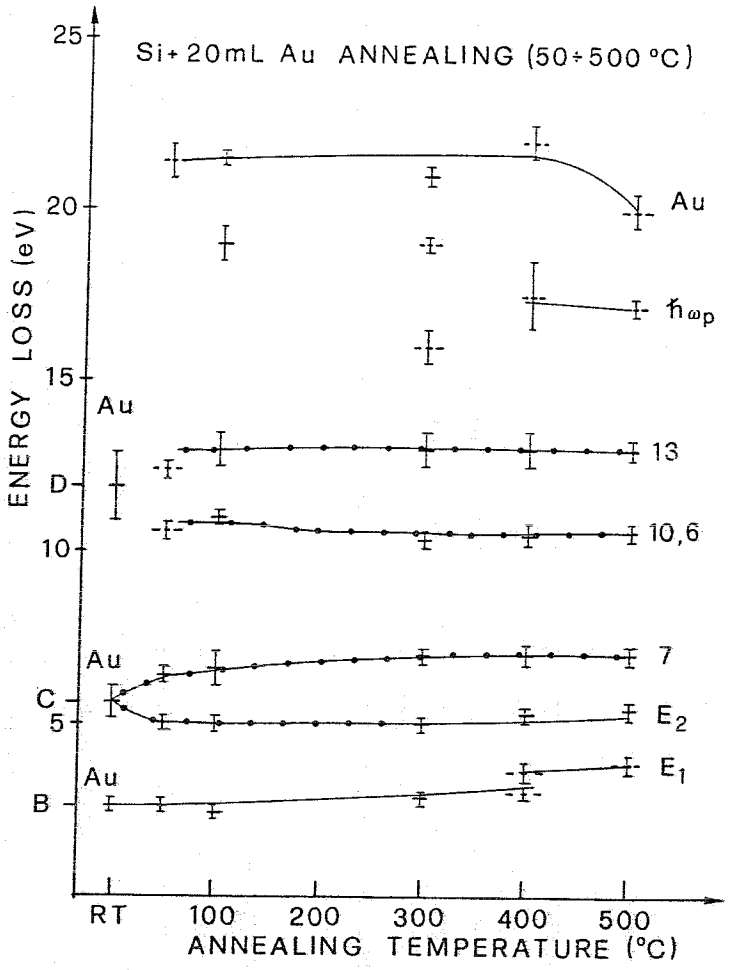

Fig. 7 - Energy position of LEELS features for θ = 20 after different annealing steps at different temperatures. Dots on full lines indicate interface losses. The feature around 5 eV becomes degenerate with the Si bulk loss E_2 and cannot be unambiguously interpreted as an interface loss nor as a Si-bulk loss.

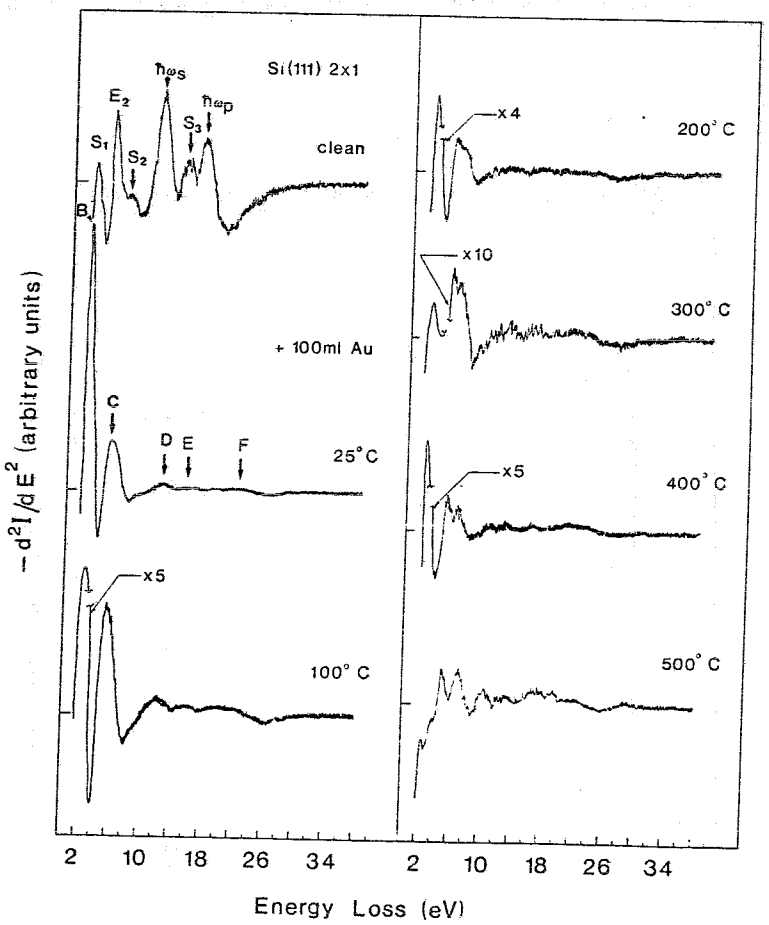

Fig. 8 - LEELS spectra for θ = 100 at RT and after different 30-minutes annealing steps at different temperatures. The top left spectrum correspond to the clean cleaved Si(111) 2x1.

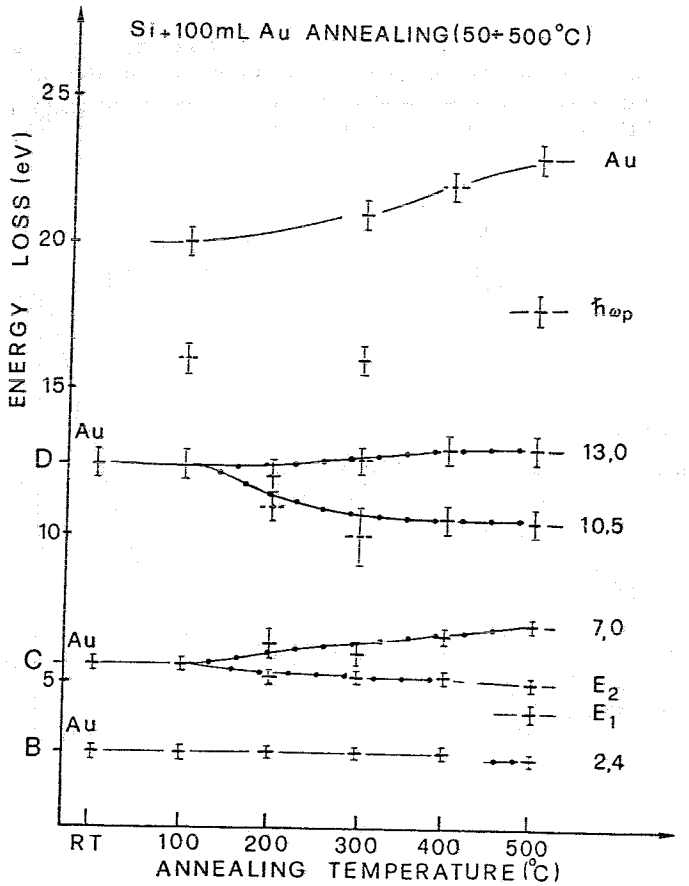

Fig. 9 - Energy positions of LEELS features for θ = 100 after different annealing steps at different temperatures. The dots have the same meaning a Fig. 7.

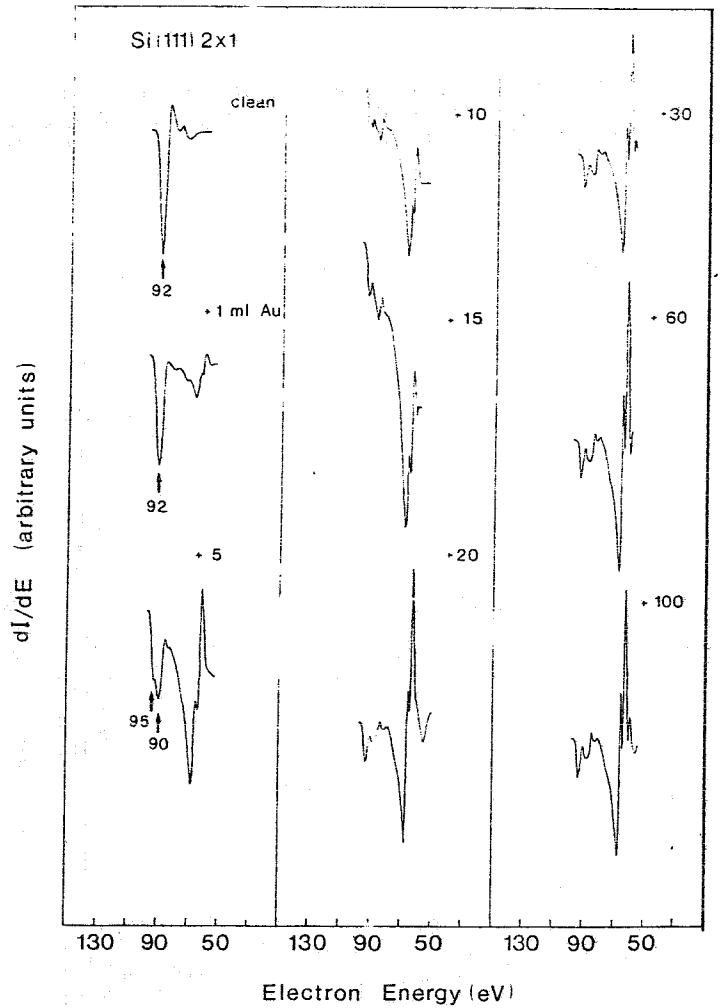

Fig. 10 - Low-energy Auger spectra of clean cleaved Si(111) 2x1 and of the same surface covered with different Au thicknesses.

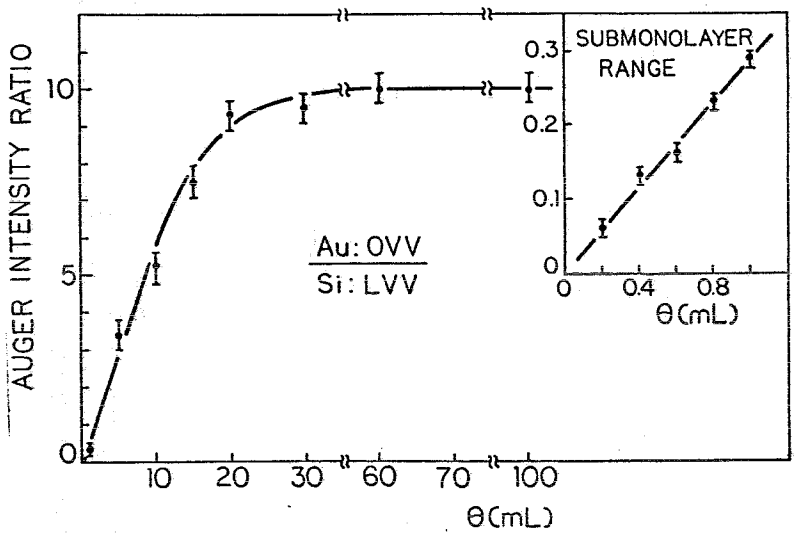

Fig. 11 - Au:OVV/Si:LVV Auger intensity vs. θ. The submonolayer-range of this plot is shown in the inset. The full line in the inset is the best fit of Eq.(6) to the experimental results.

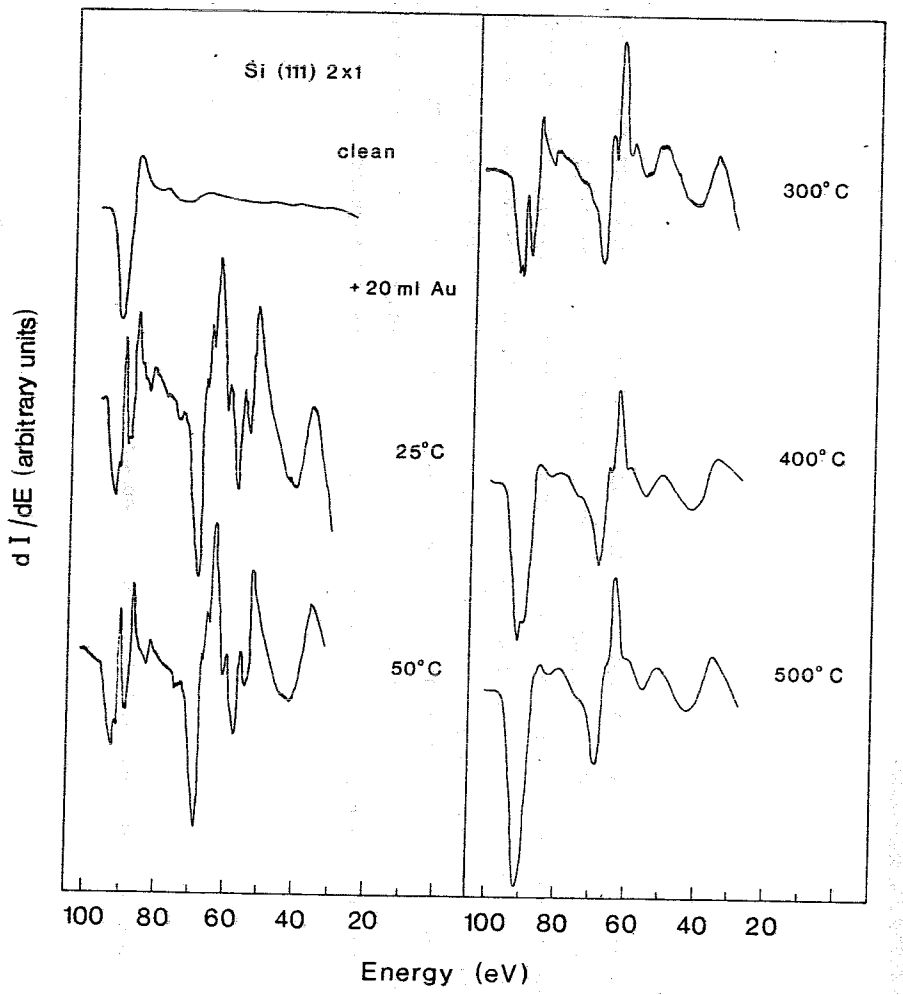

Fig. 12 - Low-energy Auger spectrum at θ = 20 and after annealing steps at different temperatures. The top left spectrum correspond to the clean cleaved Si(111) 2x1.

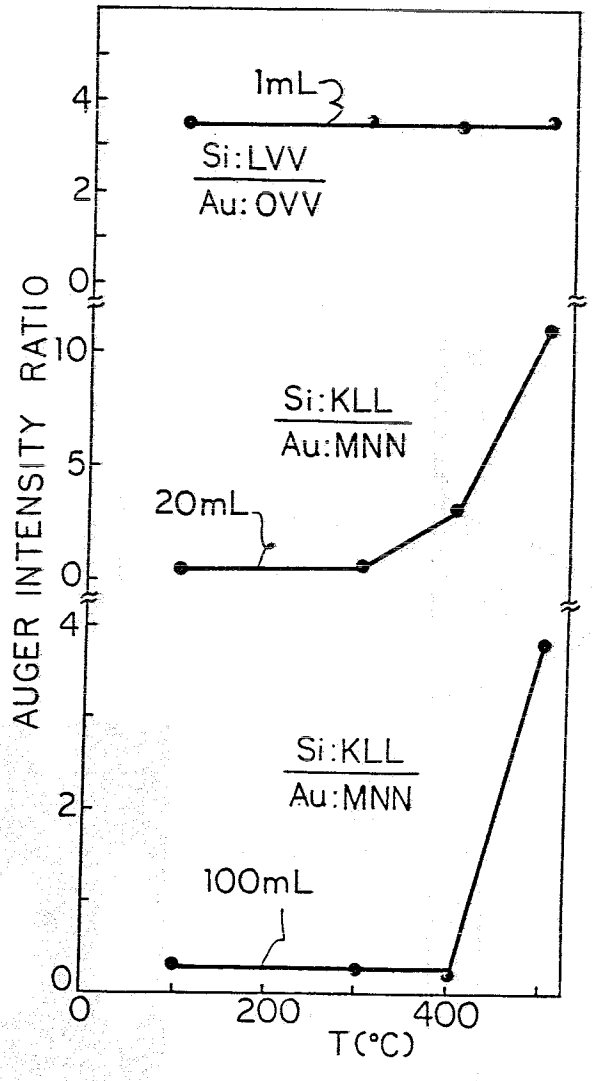

Fig. 13 - Auger lines intensity ratio, Si:KLL/Au:MNN for θ = 20, 100 and Si:LVV/Au:OVV for θ = 1, vs. annealing temperature.

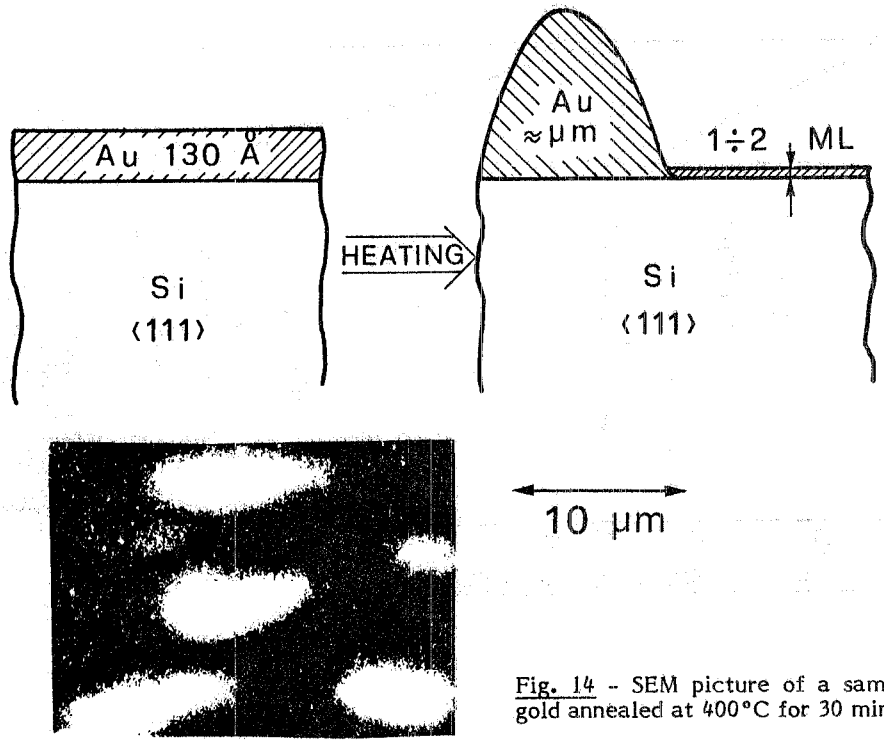

Fig. 14 - SEM picture of a sample with 100 mL of gold annealed at 400°C for 30 minutes.

4. - DISCUSSION

4.1. - Low Au coverages ($\theta \lesssim 1$)

The results reported in Sect. 3 for the low coverage range (see Fig. 2) clearly show that a small quantity of gold causes strong change in the LEELS silicon spectrum. The early appearence of the new structures I_{S1}-I_{S4} demonstrates that a reaction between silicon and gold occurs. The nature and strength of this reaction requires, however, some further analysis. For example it could be limited to the formation of Au-Si bond at an abrupt interface or it could correspond to an intermixing between the two atomic species. This analysis will be based in particular on the behavior of the Auger Au/Si intensity ratio vs. gold coverage (Fig. 11) and on the effects of the annealing cycle for θ=1 (Fig. 2). We observed in Sect. 3.2. that the silicon LVV lineshape is not affected by gold deposition in the submonolayer region--only a decrease in intensity is detected. If we use the equations

$$I_{Si} = I_{Si}^{(0)} e^{-d/L} \tag{3}$$

$$I_{Au} = I_{Au}^{(\infty)} (1-e^{-d/L}) \tag{4}$$

for the Si and Au AES intensities vs. d, the nominal Au thickness, we obtain

$$\ln(I_{Au}/I_{Si} + C) = \frac{d}{L} - \ln\frac{1}{C} \quad . \tag{5}$$

Where $I_{Si}^{(0)}$ and $I_{Au}^{(\infty)}$ are the AES intensities of the cleaved silicon and bulk gold, and $C = I_{Au}^{(\infty)}/I_{Si}^{(0)}$. The same escape

depth L has been used for both materials. This is reasonable since the Si LVV and Au OVV Auger lines have nearly the same energy. In Fig. 15 a plot of $\ln(I_{Au}/I_{Si}+C)$ is shown. We used C = 0.92 calculated from the Auger data

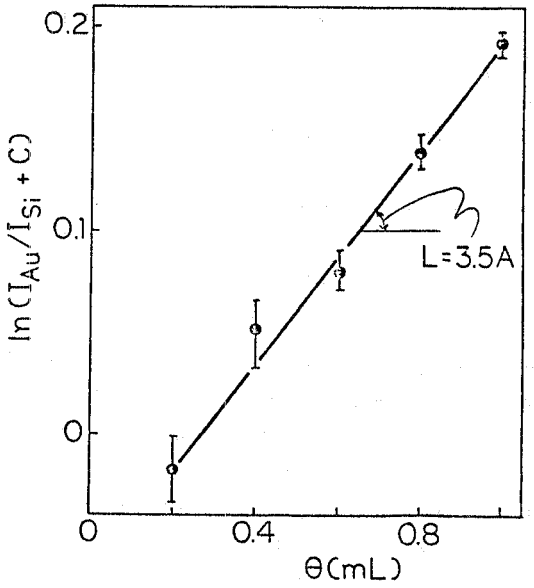

Fig. 15 - Plot of $\ln(I_{Au}/I_{Si} + C)$ vs. θ. The slope of the straight line gives an escape depth L = 3.5 A.

reported in ref.20. Small changes of C do not affect appreciably the results which follow. The plot of Fig. 15 exhibits a linear behavior and from its slope we find L = 3.5 A. For comparison the escape depth of Au at a kinetic energy of 70 eV is $\simeq 4$ A[21] and that of silicon is ≈ 5 A[22] at nearly the same kinetic energy. This shows that at $\theta \leq 1$ an abrupt junction occurs between gold and silicon. In fact a higher value of L should be obtained from eq. (3) in case of intermixing. Notice that the exponential behavior of eqs.(3) and (4) is still a good approximation in the submonolayer region. In fact for $d \rightarrow 0$:

$$I_{Au}/I_{Si} \simeq C\, d/L, \qquad (6)$$

i.e. a linear behavior. A best fit of Eq. (6) to the experimental results (inset of Fig. 11) gives L = 3.4 A. This value coincides within the experimental uncertainty with the above value L = 3.5 A. The hypothesis that at very low coverages no intermixing occurs is independently confirmed by the stability of the interface with temperature. Fig. 2 shows that an annealing cycle up to 500°C does not change the peak positions in the LEELS spectrum. Large changes are seen instead for the higher coverages (see Figs. 6 and 8). One should observe that this interface has a heat of reaction $\Delta H_R = 0$[23,24] (ΔH_R is the difference in heat of formation between bulk silicon and Si-Au complex). High negative values of ΔH_R correspond to strong reactivity between semiconductor and metal. In ref. 23, for example, link has been reported between the interface width and ΔH_R. Stronger reactivity, i.e. larger negative ΔH_R's, corresponds to thinner interfaces. In our case it seem that gold shows a different behavior at very small coverages ($\theta \leq 1$ mL). Its strong reactivity is confirmed by the Auger analysis and by the appearence of new LEELS features (Fig. 2) wich are not due to the bulk semiconductor nor to the bulk metal[25].

Similar conclusions were reached in refs. 11, 12 and 13 on the basis of Auger analysis, electron microscope observations and ion backscattering experiments. In ref. 11 a critical Au thickness limit (≈ 5 A) is reported above which the interdiffusion begins. Silicon disruption is there explained as due to the screaning by metal electrons of the Coulomb interaction between silicon atoms -- for a metal-like behavior the Au overlayer should have a thickness above 5-10 mL. This explanation, however, fails for the Si-Ag interfaces where no intermixing occurs at any Ag-coverage at RT[26]. Its validity for Si-Au is therefore questionable since these two interfaces should have

similar properties. The Si bond disruption is better explained by the formation of bonds involving Si-(sp) and gold-(sd) electrons. We shall see later that the Si-(sp)-Au-(sd) hibrid bonds in the Au-Si alloy phase are deep enough in the valence band to explain a preferential formation of Au-Si bonds. It remains to be explained why this mechanism starts after a certain Au thickness limit. From our experiments we cannot extablish exactly what this limit is. Since at θ=2 we begin to see changes in the Si-LVV Auger lineshape we estimate the limit to be approximatively 2 mL.

The loss peaks like those of Fig. 2 (peaks I_{S1} through I_{S4}) could be due in general either to single-particle excitations or to localized plasmons. In the latter case the three media, silicon, gold and vacuum can be described by the following dielectric functions[27]:

$$\varepsilon_{Si}(\omega) = 1 + \frac{\omega_{pSi}}{(\Delta^2 - \omega^2)} \quad , \qquad \varepsilon_{Au}(\omega) = 1 - \frac{\omega_{pAu}}{\omega^2} \quad , \quad \varepsilon_v = 1 \quad .$$

Where $\hbar\omega_{pSi}$ = 17 eV and $\hbar\omega_{pAu}$ = 9 eV are the bulk plasmon frequencies and Δ accounts for the deviation from the free-electron gas behavior. We are making the hypothesis that gold atoms do not interdiffuse up to 1-2 mL and that the dielectric constant of the metallic film is still that of bulk gold. Using $\varepsilon_{Si}(0) = 12$ we find $\Delta^2 = 26.3$ and the interface plasmon frequencies can be calculated from the relationships[27,29] $\varepsilon_{Si} = -\varepsilon_{Au}$ and $\varepsilon_{Au} = -1$. The three solutions are 2.3 eV, 14.3 eV and 6.4 eV respectively. Only the first one of these solutions is close to an experimental loss peak, i.e. I_{S1} peak. This indicates that mostly one-electron transitions are responsible for the new LEELS features. On the other hand the detailed nature of these transitions cannot be determined without band structure calculations.

Notice that in Figs. 2 and 3 the losses I_{S3} and I_{S4} result from an increasing splitting of the surface-plasmon peak with increasing Au coverage. This splitting can be explained by a simple model calculation[30] in the framework of the dielectric-scattering theory under the assumption that the localized gold-silicon bonds give rise to a LEELS feature nearly degenerate in energy with the surface-plasmon loss. In the energy region of interest the silicon dielectric function can be approximated by $\varepsilon_{Si}(\omega) = 1 - (\omega_p^2/\omega^2)$, where $\hbar\omega_p$ = 17 eV, and the gold-induced transition can be described by $\varepsilon_{Au,i} = A\,\omega^2_{Au,i}\,\theta/(\omega^2_{Au,i} - \omega^2 - i\omega\Gamma)$, where A, $\omega_{Au,i}$, θ and Γ are the oscillator strength parameter, gold-induced transition frequency, Au coverage and brodening parameter. Here we used a coverage-dependent oscillator strength under the reasonable assumption that increasing θ would also proportionally increase the oscillator strength of gold-related transitions. Equation (2) now becomes

$$-\mathrm{Im}\left\{1/\left[(2 - \omega_p^2/\omega^2) + A\,\omega^2_{Au,i}\,\theta/(\omega^2_{Au,i} - \omega^2 - i\omega\Gamma)\right]\right\},$$

and in the simple case of Γ=0 the $(LF)_{surface}$ has maxima when

$$2 - \frac{\omega_p^2}{\omega^2} + \frac{A\,\omega^2_{Au,i}\,\theta}{(\omega^2_{Au,i} - \omega^2)} = 0. \qquad (7)$$

A best fit of Eq. (7) to the experimental results gives the two solutions reported as dashed lines in Fig.3 with A = 0.3 and $\hbar\omega_{Au,i}$ = 11 eV.

4.2. - High Au coverages ($\theta > 1$)

A new physical situation can be inferred by the evolution of LEELS spectra for $\theta > 1$, Sect.3.1. Here more new structures are appearing (see Fig. 4) the origin of which is completely different from that of the submonolayer features. Peak B appearing at θ=5 in Fig. 4 grows simultaneously to the splitting of the Si LVV Auger peak shown in Fig. 10. The existence of this silicon doublet indicates that silicon atoms are forming new

bonds with gold atoms. The difference with the submonolayer case is that there the new structures cohexist with the bulk silicon LEELS features while at $\theta > 1$ the spectral features are characteristic of a completely new compound with no bulk-Si contributions. The splitting of Si LVV Auger line has been reported for similarly prepared systems[5-11] as well as for Si-Au alloy formed by quenching[31]. We conclude that for $\theta=5$ an intermixing has occurred between silicon and gold. Peak B in Fig. 4 is the only feature that moves in energy for increasing Au thickness. Its energy dependence is explained by a dilution of the silicon atom concentration in the Au-Si alloy for increasing θ. This dilution is inferred from the behavior of the Au:OVV/Si:LVV Auger intensity ratio, Fig. 11. A similar shift was observed[32] in the onset of interband transitions in $\varepsilon_2(\omega)$ for amorphous gold-silicon alloys of different compositions. If we locate the onset of the interband transitions at the energy for which the $\varepsilon_2(\omega)$ behaviour deviate from that of the drude equation (see Figs. 1 and 2 of ref. 32) we obtain a shift from 3.5 eV for $Au_{0.75}$ $Si_{0.25}$ to 2 eV for a nearly pure gold. The onset of interband absorption in both liquid[33] and solid[34] gold is associated with transitions from upper d-band to the Fermi level. The shift of the onset of interband transitions in the Au-Si alloys towards that of pure gold indicates that the shallowest d-electrons are those primarily involved in the bond formation with Si-(sp) electrons. This conclusion is confirmed by the shift of peak B towards its pure gold position, 2.5 eV and by its moving in energy for increasing θ's (see Fig. 4) while all other features remain unchanged. These results are in agreement with the outcomes of the theoretical calculations performed by Bisi and Calandra[35] for the cubic -phase Au_3Si, which under certain conditions has been found in thin film deposition after thermal treatment[7]. According to their conclusions the d-states, which in the pure metal lie around 2 eV below E_F, are moved to higher binding energy by hybridization with Si -(sp) states, so that the d-band in the silicide is located between 3.5 eV and 8 eV below E_F. Only minor d-structures are found in the density of states between E_F and - 3 eV. This indicate that electronic transitions involving d-states as initial states are expected to shift to lower energies upon increasing metal content in the silicides, as a consequence of increased interaction between d-states and of the minor role played by the Si-p Au-d hybrides. This trend can be related to the shift of peak B in our results (see Fig. 4) for increasing gold content in the Au-Si alloy. Similar theoretical conclusions confirmed by UPS and Auger measurements have been found by Ho et al.[36] for the Pd-Si system. We emphasize that the overall features of the chemical bonds for Pd_2Si compound are quite similar to those for the amorphous $Pd_{81}Si_{19}$ metallic glass[37]. This confirms the validity of our present approach of using theoretical results for single-crystal silicides to interpret experimental results for Si-Au alloys. A correlation can be assumed to exist between the energy position of peak B at different θ and those of the onset of interband transitions measured by optical experiments for different x composition of the $Au_{1-x}Si_x$ amorphous alloy[32]. Using this correlation we find that the first measurable energy position of B, 3.7 eV corresponds to x = 0.25, i. e. to a composition $Au_{0.75}Si_{0.25}$ close to the eutectic $Au_{0.81}Si_{0.19}$ composition. This result confirmes the hypothesis by Ottaviani et al.[38] that the eutectic composition plays an important role in the early stage of formation of metal-semiconductor interfaces. The energy shifts of peak B shown in Fig. 5 indicate that the alloy composition varies with Au thickness reaching a saturation value at $\theta \approx 20$. This value gives an estimate of the alloyed-phase thickness which agrees with the results obtained by UPS[2] and by Auger depth profiling[5-8]. Above $\theta=20$ the observed LEELS spectra becomes gold-like even though the low energy Auger spectra (Fig. 10) show the silicon doublet up to 100 mL. The saturation of the Au:OVV/Si:LVV Auger intensity ratio (Fig. 11) above $\theta \approx 20$ indicates that the silicon doublet observed up to $\theta=100$ is due to a second silicon-gold mixed phase at the outer surface. The thickness of this phase has been evaluated by Auger depth profiling[5-8] to be of the order of 1-2 monolayers. It does not affects, however, the Au-like LEELS spectrum obtained for $\theta=100$. In fact all the structures B through F may be explained by pure-gold loss function features calculated by Kramers-Kronig transform of the optical reflectivity data[39]. For comparison in Fig. 16 both $-\mathrm{Im}(1/\varepsilon(E))$ and $-\mathrm{Im}(1/\varepsilon(E)+1)$ for pure gold are reported together with the measured LEELS spectrum relative to $\theta=30$.

We have seen in Sect. 3 that the effects of the anneling are completely different for different Au overlayer

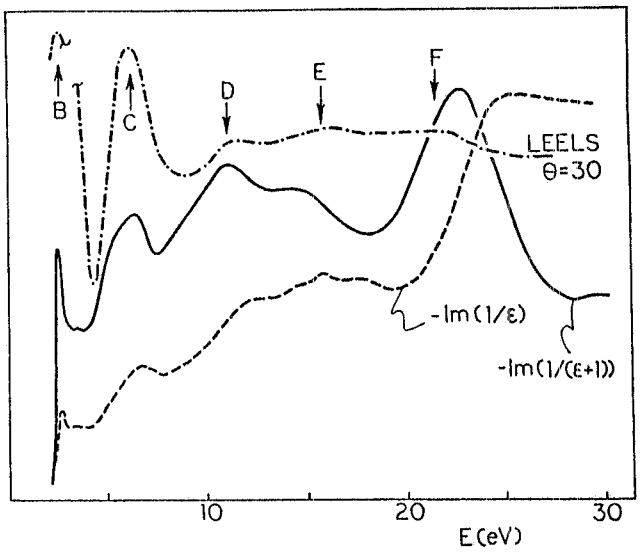

Fig. 16 - Comparison of LEELS spectrum obtained at θ = 30 with the bulk and surface loss functions of pure gold.

thicknesses. In particular we observed a strong difference between the 1 mL coverage and higher coverages. For θ = 1 the LEELS spectrum does not change with annealing. The Auger intensity ratio Si:LVV/Au:OVV (Fig. 13) also remains constant. We already emphasized that this result provides evidence for a stable electronic and structural configuration at θ = 1 coverage. On the contrary, the annealing cycles for θ = 20 and θ = 100 completely reestablish the θ = 1 LEELS spectrum. The spectra corresponding to the last step of each annealing cycle are reported in Fig. 17. The explanation for this similarity is that for high coverages the annealing process creates Au

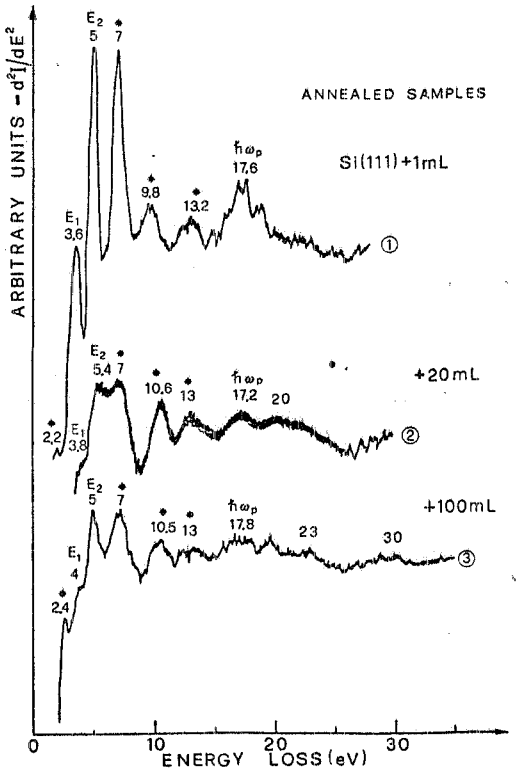

Fig. 17 - LEELS spectra obtained after the last annealing step for three different Au coverages, 1 mL, 20 mL and 100 mL. Stars indicate interface losses.

islands. The regions between islands are large in size and give the main contributions to the LEELS spectra. The structure and the electronic properties of the regions between islands are similar to those of Si covered by 1 mL of gold. The islands have been detected for θ = 100 by SEM analysis as reported in Fig. 14. The steaply rise of the

Si:KLL/Au:MNN Auger intensity ratio between T = 350°C and T 450°C reported in Fig.13 for θ = 20 and θ = 100 gives an indication of the temperature range in which the islands begin to growth. In the Au-Si phase diagram[40] the equilibrium phase is formed by pure silicon and gold separated phases. Thus the temperature effect on islands formation is due to the transition from a nonequilibrium mixed phase to the equilibrium phase. This conclusion is also evident from the low-energy Auger lineshape shown in Fig. 12. Indeed in the same temperature range the silicon doublet becomes again a single silicon peak coexisting with the gold peak.

The islands formation has been reported by Otter et al.[12] on 30 Å annealed Au films deposited on Si(111) and more recently by Tromp et al.[41] on the Si-Pd system.

5. - CONCLUSIONS.

The behavior of RT evaporated Au overlayers on Si is different for two different thickness ranges. In the submonolayer range the chemical reaction between silicon and gold atoms is strong and interface features in LEELS spectra coexist with the clean silicon structures. The persistency of all the features at the same energy loss after an annealing cycle up to 500°C toghether with the behavior of the Au:OVV/Si:LVV Auger intensity ratio indicate that the system is extremely stable and that gold do not interdiffuse with silicon at low coverage. Interface losses are interpreted as one-electron transitions. At higher coverages the splitting of Si LVV Auger peak shows that the Si-Au bond formation affects the silicon valence band states. The new situation correspond to the formation of a Si-Au alloy phase. We have shown that this phase has not a unique composition but it becomes increasingly Au-rich at larger coverages. The thickness of the alloyed phase was estimated to be $\approx$ 20 mL. Beyond this thickness essentially pure-gold grows up. The effect of annealing for high coverages shows large differences with respect to one monolayer. The LEELS spectrum changes completely and at the end of each annealing cycle all the features of the θ=1 spectrum are recovered. The evolution of the low-energy Auger peaks, of their intensity vs. annealing temperature, and a SEM analysis indicate that the annealing causes islands formation. This temperature effect is a transition from a non-equilibrium phase (alloyed phase) to an equilibrium state consisting of separated gold and silicon phases.

ACKNOWLEDGMENTS.

The authors are indebted to Prof. C.Calandra for useful discussions and for making the theoretical results on the cubic δ-phase Au_3 Si available to them prior to publication. The technical assistance of R. Bolli, M. Brolatti and the entire staff of INFN-Laboratori Nazionali di Frascati is highly appreciated.

REFERENCES

1. A.G. Milnes and P.L. Feucht, Heterojunction and Metal-semiconductor Junctions (Academic Press, New York, 1972).
2. L. Braicovich, C.M. Garner, P.R. Skeath, C.Y. Su, P.W. Chye, I. Lindau and W.E. Spicer, Phys. Rev. B20, 5131 (1980).
3. I.Abbati, L.Braicovich and A.Franciosi, Solid State Commun. 33, 881 (1980).
4. I.Abbati, L.Braicovich and A.Franciosi, Phys. Letters 80A, 69 (1980).
5. A.K.Green abd E.Bauer, J. Appl. Phys. 47, 1284 (1979).
6. G.LeLay, M.Manneville and R.Kern, Surface Sci. 65, 261 (1977).
7. T.J.Magee and J.Peng, Phys. Status Solidi (a) 49, 313 (1978).
8. K.Oura and T.Hanowa, Surface Sci. 82, 202 (1979).
9. P.Perfetti, S.Nannarone, F.Patella, C.Quaresima, A.Savoia, F.Cerrina and M.Capozi, Solid State Commun. 35, 151 (1980).
10. F.Salvan, A.Cros and J.Derrien, J. Physique Lettre 41, L-337 (1980).
11. K.Okuno, T.Ito, M.Iwami and A.Hiraki, Solid State Commun. 34, 493 (1980).
12. F.A.Otter Jr., H.C.Abbink and O.L.De Lange, Surface Sci. 27, 273 (1971).

13. T.Narusava, K.Kinoshita and W.M.Gibson, Proceedings of the Intern. Conf. on Solid Surfaces, Cannes 1980, ed. by D.D.De Gas and M.Costa (1980), Vol.I, p. 673.
14. H.Reather, Excitation of Plasmons and Interband Transitions by Electrons, Springer Tract in Modern Physics (Springer, Berlin, 1980), Vol. 88.
15. L.S.Caputi, E.Colavita, M.De Crescenzi, S.Modesti, L.Papagno, R.Scarmozzino, R.Rosei and E.Tosatti, Solid State Commun. 39, 117 (1981).
16. J.R.Rowe, G.Margaritondo and S.B.Christman, Phys. Rev. B15, 2195 (1977).
17. G.A.Sawotzky, Phys. Rev. Letters 39, 504 (1977).
18. M.Cini, Solid State Commun. 24, 681 (1977).
19. P.J.Feibelman, E.J.Mc Guire and K.C.Pandey, Phys. Rev. B15, 2202 (1977).
20. L.E.Davis, N.C.Mc Donald, P.W.Palmerg, G.E.Riach and R.E.Weber, Handbook of Auger Electron Spectroscopy (Physical Electronics Industries Inc.).
21. P.Pianetta, Ph. D. Thesis (Stanford University, Stanford, Ca., 1976), unpublished.
22. C.M.Garner, I.Lindau, C.Y.Su, P.Pianetta and W.E.Spicer, Phys. Rev. B19, 3944 (1979).
23. L.J.Brillson, C.F.Brucker, N.G.Stoffel, A.D.Katnani and G.Margaritondo, Phys. Rev. Letters 46, 838 (1981).
24. J.M.Andrews and J.C.Phillips, Phys. Rev. Letters 35, 56 (1975).
25. L.J.Brillson, Phys. Rev. Letters 40, 260 (1978).
26. See for ex.: G.Le Lay, M.Manneville and R.Kern, Surface Sci. 72, 405 (1978), and T.Hanawa and K.Oura, J. Appl. Phys. 16, 519 (1977).
27. L.J.Brillson, Phys. Rev. Letters 18, 245 (1977).
28. E.A.Stern and R.A.Ferrell, Phys. Rev. 120, 130 (1960).
29. J.W.Gadzuk, Phys. Rev. B1, 1267 (1970).
30. H.Ibach and J.E.Rowe, Phys. Rev. B9, 1951 (1974).
31. H.Hiraki and M.Iwami, Japan J. Appl. Phys. Suppl. 2, Pt. 2 (1974).
32. E.Hauser, R.J.Zirke, J.Tauc, J.J.Hauser and S.H.Nagel, Phys. Rev. Letters 40, 1733 (1978).
33. M.L.Thèye, Phys. Rev. B2, 3060 (1970).
34. N.E.Christiensen and B.O.Seraphin, Phys. Rev. B4, 3321 (1971).
35. O.Bisi, C.Calandra, I.Abbati, L.Braicovich, I.Lindau and W.E.Spicer, to be published.
36. P.S.Ho, G.W.Rubloff, J.E.Lewis, V.L.Moruzzi and A.R.Williams, Phys. Rev. B22, 4784 (1980).
37. J.D.Riley, L.Ley, J.Azoulay and K.Tarakura, Phys. Rev. B20, 776 (1979).
38. G.Ottaviani, K.N.Tu and J.W.Mayer, Phys. Rev. Letters 44, 284 (1980).
39. D.Beaglehole, M.De Crescenzi, M.L.Thèye and G.Vuye, Phys. Rev. B19, 6303 (1979).
40. M.Hansen and K.Anderko, Constitution of Binary Alloy (Mc Graw-Hill, New York, 1958).
41 R.M.Tromp, E.van Loenen, R.G.Smeenk, F.W.Saris, F.Nave and G.Ottaviani, paper presented at ECOSS 4, Munster 1981.